ChemComm

Accepted Manuscript

ROYAL SOCIETY OF CHEMISTRY

rsc.li/chemcomm

ROYAL SOCIETY OF CHEMISTRY
View Article Online
DOI: 10.1039/C9CC00206E

Chemical Communications

COMMUNICATION

Light-harvesting, 3rd generation Ru^{II}/Co^{II} MOF with large, tubular channel aperture

Received 00th October 20xx,
Accepted 00th October 20xx

DOI: 10.1039/x0xx00000x

www.rsc.org/

Luana Martins,[a] Lauren K. Macreadie,[a,b] Debobroto Sensharma,[a] Sebastien Vaesen,[a] Xia Zhang,[c] John J. Gough,[c] Mariah O' Doherty,[a] Nian-Yong Zhu,[a] Manuel Rüther,[a] John E. O'Brien,[a] A. Louise Bradley[c] and Wolfgang Schmitt[a]*

A photoactive, hetero-metallic Co^{II}/Ru^{II}-based metal-organic framework (MOF) with a large channel aperture, *ca.* 21 Å, is reported. The photophysical properties of the MOF derive from the Ru^{II} nodes giving rise to emission centred at 620 nm and relatively long triplet ^{3}MLCT lifetimes. In addition to the optical attributes, the 1*H*-imidazo [4,5-*f*][1,10]-phenanthroline ligand impart structural functionality to the MOF which is composed of alternating Co^{II}- and Ru^{II}-based nodes of Δ and Λ helicity. The framework maintains its integrity upon activation and shows gas sorption behaviour that is characteristic of mesorporous materials promoting high CO_2 sorption capacities and selectivities over N_2.

Metal-organic frameworks (MOFs) are emerging metallo-supramolecular materials with defined and controllable cavities, where inorganic nodes, i.e. metal ions or clusters, are connected through organic linkers.[1-3] Rational synthetic concepts to produce 'default' structures consider the symmetry and dimensions of both their organic and inorganic secondary building units (SBUs).[4] Many resulting framework structures are amenable to chemical functionalization, whereby possible applications derive from the intrinsic porosity, high number of active sites per unit volume and high diffusion coefficients.[5-7] These materials demonstrate how size, shape, charge and functional group availability influences guest binding and performances in gas storage, separation and catalysis.[8-10] Particularly intriguing are photoactive, '3rd or even 4th generation MOFs'[11] that can impact on areas including artificial photosynthesis,[12] photo-catalysis,[13] sensor materials,[14] light-emitting[15] or smart flexible materials.[16, 17] Considering the exceptional scientific interest in these areas, it is surprising that Ru^{II}/polypyridyl complexes have rarely been employed as SBUs of permanently porous, crystalline MOFs containing large unblocked openings.[18, 19] Ru^{II} complexes generally reveal high molar absorptivities and strongly luminesce at room temperature whereby the excited state manifold of the metal-to-ligand charge transfer (MLCT) states have intensively been investigated.[20, 21] The quantum efficiencies of the systems, *e.g.* in photo-electrochemical cells or in photocatalysis (H_2 or O_2 evolution; CO_2 reduction) rely on satisfactory excited state lifetimes and electron- and energy-transfer processes.[22]

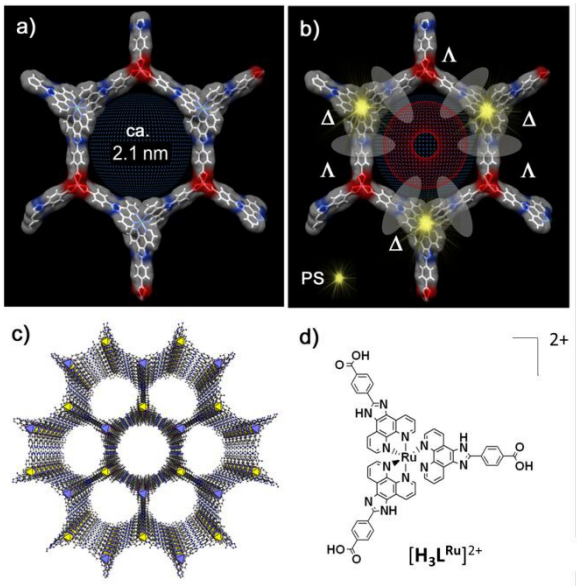

Fig. 1 Crystal structure of **Photo-MOF**; a) Hexagonal channel in [001] direction in **Photo-MOF** highlighting the aperture that is characterized by a diameter of *ca*. 21 Å. b) Key attributes of **Photo-MOF**, including Ru^{II}/phenanthroline-based photosensitisers; nodes with D_3 point symmetry of opposite helicity and imidazole-based binding sites. c) Extended structure of **Photo-MOF** with view in the direction of the crystallographic *c*-axis; d) The propeller-like metallo-ligand $[H_3L^{Ru}]^{2+}$ that directs the assembly into a hexagonal topology.

In order to preserve the polypyridyl coordination environment of Ru^{II} upon incorporation into a framework, bifunctional pyridyl-carboxylate ligands are typically used, and a bimetallic MOF is constructed using another metal centre as the structure directing unit when bound by carboxylate groups.[23,24] Generally, when Ru/pyridyl complexes or other analogous photosensitizers (PS) are incorporated into the framework structures of MOFs, quenching of the lifetime and fast energy/electron transfer processes are

[a] *School of Chemistry & CRANN Institute, University of Dublin, Trinity College, Dublin 2, Ireland. E-mail: schmittw@tcd.ie; Tel: +353-1-8963495*
[b] *CSIRO Manufacturing, Bayview Ave, Clayton, VIC 3168, Australia*
[c] *School of Physics, University of Dublin, Trinity College, Dublin 2, Ireland.*
Supplementary Information (ESI) available: Experimental and crystallographic data in CIF format for the structures. See DOI: 10.1039/x0xx00000x

observed.[25-27] Such quenching effects are desirable for several applications, including heterogeneous oxidation/reduction catalysis at secondary catalytic nodes or for dye-sensitised solar cell fabrication.[28-30] The significance of {Ru/pyridyl} nodes as hopping intermediates for energy transfer has been demonstrated using Zn(II)-containing MOFs.[27] Further, noteworthy are UiO-type MOFs in which Ru- or Ir/pyridyl nodes connect $\{Zr_6O_4(OH)_4(CO_2)_{12}\}$ units and that can be applied for the photocatalytic CO_2 reduction and the oxidation of organic substrates.[31] Similarly Ru(II)/Eu(II)-based MOFs can be applied as photosensitizing materials for CO_2 reduction.[25]

Here, we report a photoactive, '3rd generation' MOF, $[Co^{II}\mathbf{L^{Ru}}]$TFA (**Photo-MOF**) and that is characterised by accessible, tubular 1D channels with a large pore aperture. The synthetic approach employs the racemic propeller-like metallo-ligand $[\mathbf{H_3L^{Ru}}]^{2+}$ that directs the assembly into a honeycomb, **hcb** topology with alternating Co^{II}- and Ru^{II}-based nodes of Δ and Λ helicity. Interestingly, the light-harvesting and emission spectral properties of the metallo-ligands are maintained in the framework structure, and significant lifetime quenching observed. **Photo-MOF** reveals structural stability, permanent porosity and shows selectivity for CO_2 over N_2. It is further noteworthy that the incorporation of the PS results in an increased photo-stability of **Photo-MOF** in comparison to $[\mathbf{H_3L^{Ru}}](PF_6)_2$.

The tritopic Ru^{II} metallo-ligand $[\mathbf{H_3L^{Ru}}]^{2+}$ featuring a carboxylate-derivative of 1*H*-imidazo [4,5-*f*][1,10]-phenanthroline, was synthesised in two steps involving the coordination of 1,10-phenanthroline-5,6-dione to $Ru(DMSO)_4Cl_2$ followed by a Debus-Radziszewski reaction to introduce the phenylcarboxylate functionality (ESI, Scheme S1-S3).[32] The identity of $[\mathbf{H_3L^{Ru}}]^{2+}$ was confirmed by ^1H, ^{13}C and ^{13}C ^1H-COSY NMR analysis that gives rise to signals corresponding to the aromatic phenanthroline and imidazole moieties (ESI, Fig. S1-S3). **Photo-MOF** forms reproducibly under solvothermal conditions in DMF at 120 °C during the reaction between $[\mathbf{H_3L^{Ru}}]^{2+}$ and Co^{II} salts at a mole ratio of 1:10 in the presence of trifluoroacetic acid (HTFA). Single-crystal X-ray studies demonstrate (Table S1) that **Photo-MOF** crystallizes in the trigonal space group $P\bar{3}1c$, whereby the asymmetric unit comprises of 1/6 of the Ru(II) and Co(II) atoms and ½ of the organic ligand derivative. The homoleptic Ru^{II} complex $[\mathbf{L^{Ru}}]^-$ is maintained in the framework structure whereby each carboxylate moiety links to a Co^{II} centre (Fig. 1). The Co^{II} centres in **Photo-MOF** adopt octahedral coordination environments, each coordinated by three bidentate, chelating carboxylate functionalities that derive from three different $[\mathbf{L^{Ru}}]^-$ SBUs. Thus, the tris-bidentate coordination geometry of both, the {Co^{II}/carboxylate} and {Ru^{II}/phenanthroline} SBUs, results in structurally similar nodes with D_3 point group symmetry that can be resolved into Δ and Λ enantiomers depending on their helicity. The extended structure results in 2D hexagonal layers composed of alternating Co^{II} and Ru^{II} nodes of opposite handedness. The layers pack in the direction of the crystallographic *c*-axis in an *ABAB* fashion, involving π-CH and π-NH interactions to form hexagonal channels. Particularly noteworthy is the large channel aperture that is characterised by cross-sectional diameters of *ca.* 21 Å which is ideal for encapsulation and rapid diffusion of guest molecules. The stereochemistry of the individual nodes and the geometry of the channels are characterised by the symmetry operation of an improper S_3 axis which coincides with the centre of the channels and combines the C_3 rotation with a reflection through a plane perpendicular to this rotational axis. The phase-purity of the MOF was confirmed by powder X-ray

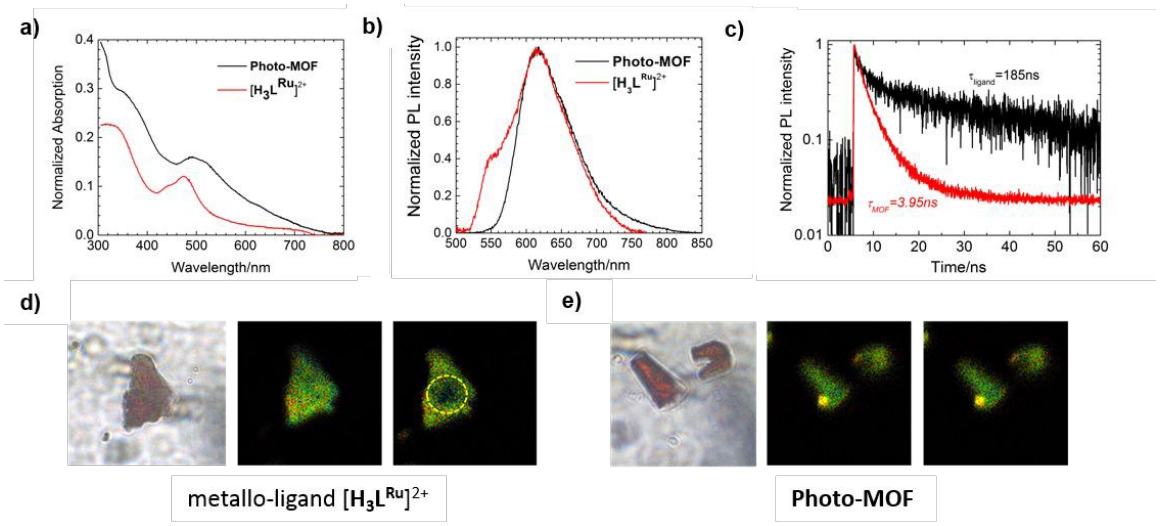

Fig. 2 Optical characterisation of **Photo-MOF** and $[\mathbf{H_3L^{Ru}}](PF_6)_2$. Details of the measurement parameters are given in the ESI; a) Normalised absorption spectra of **Photo-MOF** and $[\mathbf{H_3L^{Ru}}](PF_6)_2$ dispersed in DMF; (b) Normalised photoluminescence (PL) spectra of **Photo-MOF** and $[\mathbf{H_3L^{Ru}}](PF_6)_2$ in DMF (λ_{ex} = 405 nm); c) Normailised time-resolved photoluminescence (TRPL) decays of **Photo-MOF** and $[\mathbf{H_3L^{Ru}}]^{2+}$ in DMF measured over 50 ns with a 40 nm bandpass filter centred at 600 nm (λ_{ex}= 405 nm; excitation power 160 nW for the and $[\mathbf{H_3L^{Ru}}](PF_6)_2$ and 2.9 microWatt for the Photo-MOF).; d) and e) Optical and fluorescence-lifetime imaging microscopy (FLIM) images of solid state $[\mathbf{H_3L^{Ru}}](PF_6)_2$ and solid state **Photo-MOF** before and after excitation with 4 microWatt excitation at 405 nm, respectively. The FLIM images are in false-colour with each colour representing a lifetime, and the brightness of the colour representing the intensity. The FLIM images are measured using λ_{ex} = 405 nm; scan time: 300 s; spot-size *ca.* 430 nm. The damaged area for $[\mathbf{H_3L^{Ru}}](PF_6)_2$ is the highlighted by yellow circle.

diffraction experiments (ESI, Fig. S4). Solid-state ^{13}C and ^{19}F NMR experiments confirm the paramagnetic nature of the **Photo-MOF** and indicate that discorded TFA ions act as potential counterions (ESI Fig. S5-S7).

To evaluate the role of the PS, UV-Vis absorption, spectral photoluminescence (PL) and time-resolved photoluminescence (TRPL) studies were performed using both $[\mathbf{H_3L^{Ru}}](PF_6)_2$ and **Photo-MOF** (Fig. 2). Details of the measurement systems and parameters are provided in ESI (Section S3). The studies demonstrate that the key spectral attributes of $[\mathbf{H_3L^{Ru}}]^{2+}$ are maintained in **Photo-MOF**. Bands in the UV-Vis absorption spectra are characteristic for {Ru/phenanthroline} species giving rise to ligand-centred transitions at *ca.* 200 – 300 nm (Fig. 2a).[33, 34] Broad absorbance bands at *ca.* 480 nm can be assigned to ^{1}MLCT transitions and demonstrate that excitation energies of the chromophore are only slightly altered in **Photo-MOF** in comparison to the metallo-ligand.[35-37] The PL spectrum of **Photo-MOF** dispersed in DMF is centred at approximately 620 nm and shows evidence of a stronger shoulder on the lower wavelength side of the spectrum when compared to $[\mathbf{H_3L^{Ru}}]^{2+}$ (Fig. 2b) as a result of the incorporation of the Co^{II} ions. TRPL experiments were also performed on **Photo-MOF** and $[\mathbf{H_3L^{Ru}}](PF_6)_2$ in DMF (Fig. 2c). TRPL decays (recorded at λ_{emis}= 600 nm with an excitation power of 20 nW) for $[\mathbf{H_3L^{Ru}}]^{2+}$ and **Photo-MOF** are shown in Fig. 2c and highlight the reduced PL decay lifetime for **Photo-MOF**. TRPL decays measured using three bandpass filters with centre wavelengths across the PL spectra reveal that the lifetime of the ^{3}MLCT state of $[\mathbf{H_3L^{Ru}}]^{2+}$ is consistently reduced upon coordination to Co^{II} ions in **PhotoMOF** (ESI Fig. S8) The studies emphasise that the native photophysical properties of $[\mathbf{H_3L^{Ru}}]^{2+}$ are maintained in **Photo-MOF**, whereby coordination to Co^{II} ions gives rise to electron/energy transfer processes throughout the network structure. This is consistent with a predominant Dexter mechanism for energy transfer in MOFs.[18, 27]

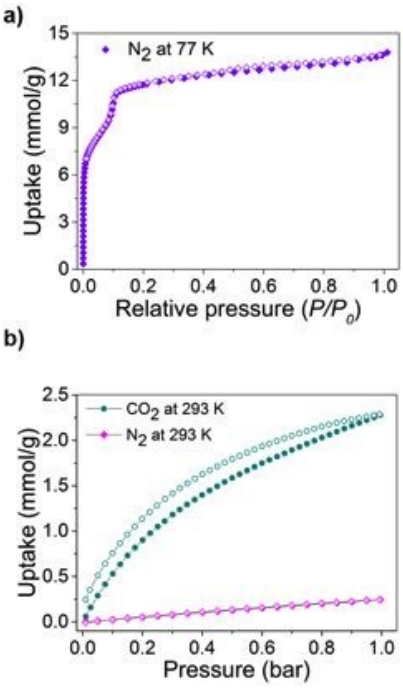

Fig. 3 a) N_2 adsorption isotherm (filled diamonds) and desorption (empty diamonds) using **Photo-MOF** at 77 K; *Inset*: Pore-size distribution of **Photo-MOF** calculated by DFT method b) CO_2 (circles) and N_2 (diamonds) sorption isotherms of **Photo-MOF** measured at 293 K; adsorption: filled symbols; desorption: empty symbols.

Fluorescence lifetime imaging microscopy (FLIM) was applied to solid-state samples to demonstrate the uniform distribution of fluorophores within the material and evaluate the opto-thermal stability of **Photo-MOF**. Interestingly, whilst the solid material of $[\mathbf{H_3L^{Ru}}](PF_6)_2$ undergoes rapid degradation upon exposure to the higher power laser excitation, no detectable damage is noticed for crystals of **Photo-MOF**. This can be attributed to the lower density of chromophores per unit volume and possibly the inherent structural integrity or the heat dissipation (Fig. 2d and e).

Thermogravimetric analysis under N_2 flow (ESI, Fig. S9) reveals good thermal stability of the MOF. A weight loss of *ca.* 46 % between 20 and 100 °C can be attributed to the removal of constitutional solvent molecules. The framework structure undergoes decomposition above 250 °C. N_2 adsorption at 77 K (Fig. 3a; ESI S10) confirmed structural integrity upon activation which involved solvent-exchange using methanol followed by thermal activation at 150 °C for 12 hours under secondary vacuum. The Brunner-Emmett-Teller (BET) surface area was found to be *ca*. 910 m^2/g and total pore volume of 0.478 cm^3/g was determined (ESI; Fig. S13). The adsorption-desorption isotherms reveal type IV(b) behaviour, characterized by rather steep adsorption at low relative pressures followed by a step at a relative pressure of 0.1 whereby no hysteresis effects are observed.[38, 39]

The characteristic step is consistent with the presence of small mesopores of *ca.* 2 nm in diameter, as confirmed by structural analysis and DFT estimations (ESI, Fig. S15), in which capillary condensation of N_2 takes place.[40] Further CO_2 and N_2 adsorption isotherms were measured at 293 K (Fig. 3b; ESI Fig. S16). **Photo-MOF** adsorbs CO_2 and N_2 reversibly, indicating that no chemisorption processes prevail under the applied conditions. The adsorption storage capacities at 1 bar for CO_2 and N_2 are 2.28 mmol/g and 0.244 mmol/g, respectively. Thus **Photo-MOF** reveals a CO_2/N_2 selectivity of 26.7 suggesting preferential CO_2-framework interactions within the 1-D channels of **Photo-MOF** (e.g. interactions with the imidazole functionality of the organic ligands, see also ESI, Fig. S16; Table S2).[41]

In conclusion, **Photo-MOF** represents a permanently porous, photoactive, hetero-metallic MOF with accessible helical 1D channels. Despite its large pore aperture, the framework maintains its structural integrity and shows gas sorption behaviour that is characteristic of mesoporous materials. Its structural attributes promote relatively high CO_2 storage capacities and selectivity over N_2. Importantly, the MOF maintains the photo-physical properties of the Ru^{II} nodes whereby the ^{3}MLCT lifetime is reduced upon coordination to Co^{II} ions giving rise to electron/energy transfer processes throughout the network structure. The 1*H*-imidazo [4,5-*f*][1,10]-phenanthroline ligand imparts further functionality to the racemic framework structure which is composed of alternating Co^{II}- and Ru^{II}-based nodes of Δ and Λ helicity. These

attributes, combining unique structural and optical attributes, render **Photo-MOF** as a highly intriguing material for future photo-catalysis and photo-electrochemical studies that extends the library of '3rd -generation' photoactive MOFs.

The authors thank the Brazilian National Council for Scientific and Technological Development (CNPq), Science Foundation Ireland (13/IA/1896) and the European Research Council (CoG 2014–647719) for the financial support. We thank Dr. B. Twamley for the X-ray diffraction measurements.

Notes and references

1. S. R. Batten, N. R. Champness, X.-M. Chen, J. Garcia-Martinez, S. Kitagawa, L. Öhrström, M. O'Keeffe, M. Paik Suh and J. Reedijk, *Pure Appl. Chem.*, 2013, **85**, 1715.
2. S. R. Batten, N. R. Champness, X.-M. Chen, J. Garcia-Martinez, S. Kitagawa, L. Öhrström, M. O'Keeffe, M. P. Suh and J. Reedijk, *CrystEngComm*, 2012, **14**, 3001.
3. S. Kitagawa, R. Kitaura and S.-i. Noro, *Angew. Chem. Int. Ed.*, 2004, **43**, 2334.
4. O. M. Yaghi, M. O'Keeffe, N. W. Ockwig, H. K. Chae, M. Eddaoudi and J. Kim, *Nature*, 2003, **423**, 705.
5. S. Han, T. M. Hermans, P. E. Fuller, Y. Wei and B. A. Grzybowski, *Angew. Chem. Int. Ed.*, 2012, **51**, 2662.
6. O. K. Farha, I. Eryazici, N. C. Jeong, B. G. Hauser, C. E. Wilmer, A. A. Sarjeant, R. Q. Snurr, S. T. Nguyen, A. O. z. r. Yazaydın and J. T. Hupp, *J. Am. Chem. Soc.*, 2012, **134**, 15016.
7. H. Deng, S. Grunder, K. E. Cordova, C. Valente, H. Furukawa, M. Hmadeh, F. Gándara, A. C. Whalley, Z. Liu, S. Asahina, H. Kazumori, M. O'Keeffe, O. Terasaki, J. F. Stoddart and O. M. Yaghi, *Science*, 2012, **336**, 1018.
8. L. R. MacGillivray, John Wiley & Sons, 2010, pp. 165.
9. J. Lee, O. K. Farha, J. Roberts, K. A. Scheidt, S. T. Nguyen and J. T. Hupp, *Chem. Soc. Rev.*, 2009, **38**, 1450.
10. I. Nath, J. Chakraborty and F. Verpoort, *Chem. Soc. Rev.*, 2016, **45**, 4127.
11. C. S. Diercks, Y. Liu, K. E. Cordova and O. M. Yaghi, *Nat. Mater.*, 2018, **17**, 301.
12. T. Zhang and W. Lin, *Chem. Soc. Rev.*, 2014, **43**, 5982.
13. J.-L. Wang, C. Wang and W. Lin, *ACS Catal.*, 2012, **2**, 2630.
14. E. A. Dolgopolova, A. M. Rice, C. R. Martin and N. B. Shustova, *Chem. Soc. Rev.*, 2018, 4710.
15. E. Feijó de Melo, N. d. C. Santana, K. G. Bezerra Alves, G. F. de Sá, C. Pinto de Melo, M. O. Rodrigues and S. A. Júnior, *J. Mater. Chem.*, 2013, **1**, 7574.
16. H. Li and M. R. Hill, *Acc. Chem. Res.*, 2017, **50**, 778-786.
17. X. Zhao, X. Song, Y. Li, Z. Chang and L. Chen, *ACS Appl. Mater. Interfaces*, 2018, **10**, 5633.
18. M. C. So, G. P. Wiederrecht, J. E. Mondloch, J. T. Hupp and O. K. Farha, *Chem. Commun.*, 2015, **51**, 3501.
19. J. Yu, X. Li and P. Deria, *ACS Sustainable Chem. Eng.*, 2018, **7**, 1841-1854.
20. A. Juris, V. Balzani, F. Barigelletti, S. Campagna, P. Belser and A. von Zelewsky, *Coord. Chem. Rev.*, 1988, **84**, 85.
21. S. Campagna, F. Puntoriero, F. Nastasi, G. Bergamini and V. Balzani, in *Photochemistry and Photophysics of Coordination Compounds I*, Springer, 2007, pp. 117.
22. D. M. Arias-Rotondo and J. K. McCusker, *Chem. Soc. Rev.*, 2016, **45**, 5803.
23. A. Santiago-Portillo, H. G. Baldoví, E. Carbonell, S. Navalón, M. Álvaro, H. García and B. Ferrer, *J. Phys. Chem. C*, 2018, **122**, 29190.
24. W. A. Maza, S. R. Ahrenholtz, C. C. Epley, C. S. Day and A. J. Morris, *J. Phys. Chem. C*, 2014, **118**, 14200.
25. Z.-H. Yan, M.-H. Du, J. Liu, S. Jin, C. Wang, G.-L. Zhuang, X.-J. Kong, L.-S. Long and L.-S. Zheng, *Nat. Commun.*, 2018, **9**, 3353.
26. H.-J. Son, S. Jin, S. Patwardhan, S. J. Wezenberg, N. C. Jeong, M. So, C. E. Wilmer, A. A. Sarjeant, G. C. Schatz, R. Q. Snurr, O. K. Farha, G. P. Wiederrecht and J. T. Hupp, *J. Am. Chem. Soc.*, 2013, **135**, 862.
27. C. A. Kent, B. P. Mehl, L. Ma, J. M. Papanikolas, T. J. Meyer and W. Lin, *J. Am. Chem. Soc.*, 2010, **132**, 12767.
28. K. Leong, M. E. Foster, B. M. Wong, E. D. Spoerke, D. Van Gough, J. C. Deaton and M. D. Allendorf, *J. Mater. Chem.*, 2014, **2**, 3389.
29. S. Jin, H.-J. Son, O. K. Farha, G. P. Wiederrecht and J. T. Hupp, *J. Am. Chem. Soc.*, 2013, **135**, 955.
30. W. A. Maza, A. J. Haring, S. R. Ahrenholtz, C. C. Epley, S. Y. Lin and A. J. Morris, *Chem. Sci.*, 2016, **7**, 719.
31. C. Wang, Z. Xie, K. E. deKrafft and W. Lin, *J. Am. Chem. Soc.*, 2011, **133**, 13445.
32. H. Debus, *Justus Liebigs Annalen der Chemie*, 1858, **107**, 199..
33. A. K. Mengele, S. Kaufhold, C. Streb and S. Rau, *Dalton Trans.*, 2016, **45**, 6612.
34. R. Staehle, C. Reichardt, J. Popp, D. Sorsche, L. Petermann, K. Kastner, C. Streb, B. Dietzek and S. Rau, *Eur. J. Inorg. Chem.*, 2015, **2015**, 3932..
35. I. M. M. de Carvalho, Í. de Sousa Moreira and M. H. Gehlen, *Polyhedron*, 2005, **24**, 65.
36. M. Schwalbe, B. Schäfer, H. Görls, S. Rau, S. Tschierlei, M. Schmitt, J. Popp, G. Vaughan, W. Henry and J. G. Vos, *Eur. J. Inorg. Chem.*, 2008, **2008**, 3310.
37. W. F. Wacholtz, R. A. Auerbach and R. H. Schmehl, *Inorg. Chem.*, 1986, **25**, 227.
38. M. Thommes, K. Kaneko, A. V. Neimark, J. P. Olivier, F. Rodriguez-Reinoso, J. Rouquerol and K. S. Sing, *Pure Appl. Chem.*, 2015, **87**, 1051.
39. K. A. Cychosz and M. Thommes, *Engineering*, 2018, **4**, 559.
40. J. Rouquerol, D. Avnir, C. Fairbridge, D. Everett, J. Haynes, N. Pernicone, J. Ramsay, K. Sing and K. Unger, *Pure Appl. Chem.*, 1994, **66**, 1739.
41. R. A. Agarwal and N. K. Gupta, *Coord. Chem. Rev.*, 2017, **332**, 100.

View Article Online
DOI: 10.1039/C9CC00206E

Graphical Abstract

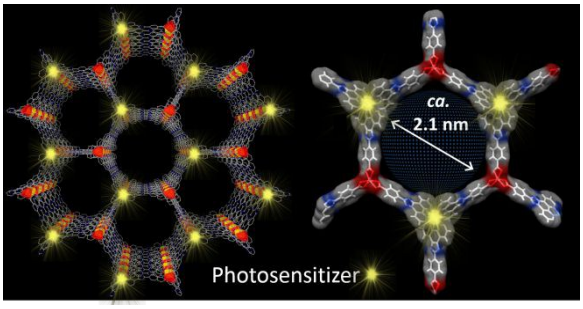

Table of Contents entry:

View Article Online
DOI: 10.1039/C9CC00206E

A photoactive Co^{II}/Ru^{II}-based MOF with a channel aperture of *ca.* 21 Å is reported; its gas sorption behavior is characteristic for mesoporous materials with CO_2 sorption selectivity over N_2.